This is the post-print (i.e. final draft post-refereeing) of the publication.
The final publication is available at Elsevier via http://dx.doi.org/10.1016/j.jeurceramsoc.2016.03.022

Extensive domain wall contribution to strain in a (K,Na)NbO_3-based lead-free piezoceramics quantified from high energy X-ray diffraction

Diego A. Ochoa[a,b], Giovanni Esteves[b], Thanakorn Iamsasri[b], Fernando Rubio-Marcos[c], José F. Fernández[c], Jose E. García[a,*], Jacob L. Jones[b]

[a] *Department of Physics, Universitat Politècnica de Catalunya - BarcelonaTech, Barcelona 08034, Spain*
[b] *Department of Materials Science and Engineering, North Carolina State University, Raleigh, North Carolina 27696, USA*
[c] *Department of Electroceramics, Instituto de Cerámica y Vidrio, CSIC, Madrid 28049, Spain*

Abstract

The origins of high piezoelectric properties in the lead-free (K,Na)NbO_3-based tetragonal composition $(K_{0.44}Na_{0.52}Li_{0.04})(Nb_{0.86}Ta_{0.10}Sb_{0.04})O_3$ (KNL-NTS) is investigated by quantifying the intrinsic and extrinsic contributions from high energy X-ray diffraction measurements. The applied methodology, which allows discerning between the intrinsic contribution, related to the field induced lattice distortion, and the extrinsic contributions, related to non-180° domain wall motion, is widely described in this work. The non-180° domain reorientation of the KNL-NTS piezoceramic is quantify from the integrated intensities of the 002 and 200 reflections obtained from line profile, while the shifts in peak position versus the applied electric field is used to obtain the lattice strain contribution. Large non-180° domain wall contribution to the electric field induced macroscopic strain (~80% of the macroscopic strain) is verified in KNL-NTS.

Keywords: piezoceramics, ferroelectrics, X-ray diffraction, KNN, domain walls

* Corresponding author at: Department of Physics, Universitat Politècnica de Catalunya, Jordi Girona 1-3, modul B4, 08034 Barcelona, Spain.
E-mail address: jose.eduardo.garcia@upc.edu (J.E. García).

1. Introduction

Lead-free piezoelectric polycrystals have recently attracted attention due to their significant reduction in toxicity compared to the leading piezoelectric material, lead zirconate titanate (PZT) [1]. Finding lead-free piezoelectric polycrystals with high performance properties has proven to be a challenge because most lead-free systems show low piezoelectric response. A potential candidate that exhibits high piezoelectric properties, comparable to PZT, is the $(K,Na,Li)(Nb,Ta,Sb)O_3$ (KNL-NTS) system. The high piezoelectric response of the KNL-NTS system is associated with the proximity of the polymorphic phase boundary (PPB) to room temperature [2]. This system has received much attention due to a study done by Saito *et al.* [2] reporting d_{33} values of ~300 pC/N and ~450 pC/N for randomly oriented and textured polycrystals, respectively. An optimized lead-free composition could prove beneficial to many applications that utilize piezoelectric materials such as transducers, transformers, ultrasonic motors, and medical applications where lead cannot be present [3].

The piezoelectric coefficients are comprised of both intrinsic and extrinsic contributions. The intrinsic contribution, related to the field induced lattice distortion, is associated with the change in the polarization of the unit cell either through polarization extension or polarization rotation [4]. The extrinsic contribution, on the other hand, is mainly associated with the domain wall configuration and motion. Domain walls can be categorized as either 180° or non-180° domain walls. The types of non-180° domain walls depend on the crystal structure of the material, for instance 90º domain walls are found in tetragonal perovskite ferroelectrics. The extrinsic contribution is known to be the most significant contribution to the macroscopic piezoelectric properties at room temperature in the PZT system [5].

In the present work, the intrinsic and extrinsic contributions to the macroscopic piezoelectric response are investigated in KNL-NTS in order to gain insights on the mechanisms related to these responses, and enable the enhancement of the piezoelectric properties of lead-free piezoceramics in the future. In order to avoid complexity of the mixture of phases, a single phase tetragonal $(K_{0.44}Na_{0.52}Li_{0.04})(Nb_{0.86}Ta_{0.10}Sb_{0.04})O_3$ sample is used for the performed study. The contribution of non-180° domain wall motion to macroscopic strain of KNL-NTS is calculated using *in situ* X-ray diffraction (XRD). XRD is a versatile technique to study the average structural and crystallographic response to applied electric fields in piezoelectric materials. The ferroelastic domains reorientation can be quantify from the integrated intensities of degenerate reflections, such as the 002 and 200 in a tetragonal material, obtained from line profile analysis [6,7]. The XRD data processing enables the quantification of the lattice strain and the extrinsic strain exerted by the sample and gives insight into the correlation between the microstructure and the macroscopic strain. By using the calculated strain arising from non-180° domain wall motion and comparing the results to the macroscopic strain measurements, the main contribution to the macroscopic strain can be elucidated. The results of this work can help further advance the ferroelectric properties of lead-free piezoceramics, which are more environmentally and biologically friendly.

2. Experimental procedure

2.1. Sample preparation

The $(K_{0.44}Na_{0.52}Li_{0.04})(Nb_{0.86}Ta_{0.10}Sb_{0.04})O_3$ sample was synthesized by conventional solid-state processing, which is described in detail in Ref. [8]. The sample was sintered at 1125°C for 16 hours. The density of the sintered sample is 4.69 g/cm^3 (98% of the theoretical density). The

material microstructure consists of faceted grains with a bimodal grain size distribution having equivalent diameters of 1 and 3 μm, respectively (the reader can find more information about the microstructural characterization in the Supplementary Material). The room temperature XRD measurement, shown in Fig. 1, confirms that the sample has a tetragonal crystal structure and an analysis using the Rietveld method confirms the pattern can be modeled well using the space group *P*4*mm*.

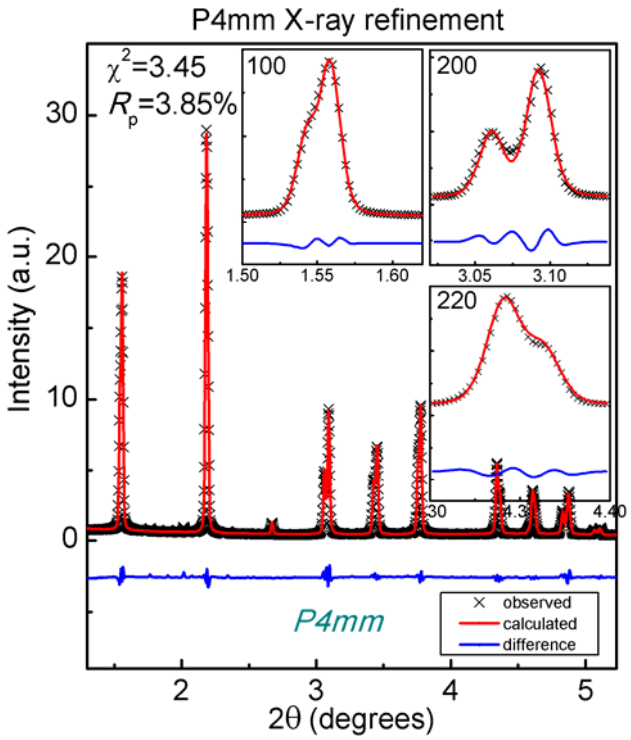

Fig. 1. High energy XRD Rietveld refinement using a P4mm tetragonal symmetry for KNL-NTS at room temperature.

2.2. Measurement methods

Diffraction patterns were measured during application of electric fields using high energy X-rays at beamline 11-ID-C of the Advanced Photon Source at Argonne National Laboratory. The sample was placed onto a stage designed for electric field application, and irradiated in

transmission mode using an X-ray beam with a wavelength of 0.10798 Å, and 0.5 mm × 0.5 mm in size. A cerium dioxide (NIST 674b) standard was used to calibrate sample to detector distance, beam center, and detector orthogonality for data reduction from two-dimensional (2D) XRD patterns using the *Fit2D* program [9]. The sample was subjected to an electric field amplitude of 2 kV/mm utilizing a triangular bipolar waveform with a frequency of 0.0125 Hz. The software available at the 11-ID-C beamline allowed for time synchronization of the diffracted X-ray beam with applied voltage, thus allowing the material response to be captured at the specified frequency. A simplified diagram of the how the sample is measured and data collected is shown in Fig. 2.

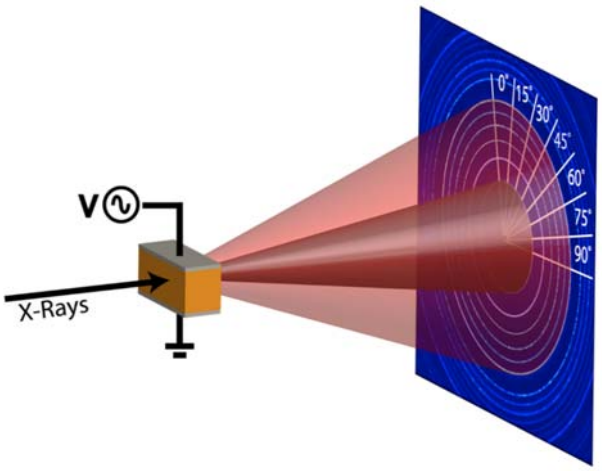

Fig. 2. Experimental XRD setup. 2D diffraction patterns are obtained during the application of electric field. Incident high energy x-rays are perpendicular to the applied electric field.

The macroscopic strain-electric field hysteresis loop was measured using a Hewlett-Packard 33120A signal generator, a Trek 663 signal amplifier, and a WayCon inductive position transducer conditioning with a Solartron OD5 Module. A schematic setup is shown in Fig. 3. A sinusoidal signal with a frequency of 0.1 Hz and amplitude 2 kV/mm was applied to the sample.

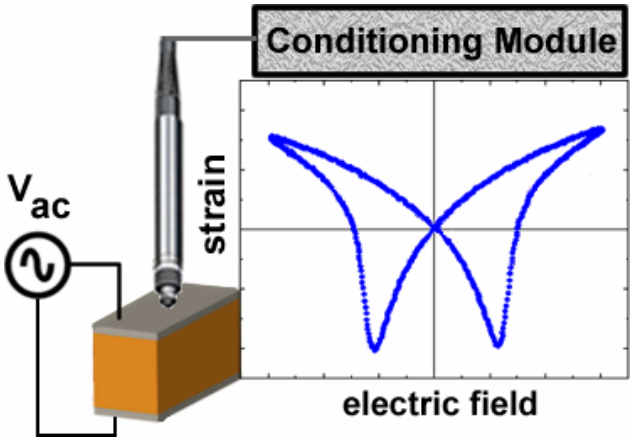

Fig. 3. Experimental setup to measure strain versus electric field (S-E) hysteresis loop. The strain (S) is measured using an inductive position transducer properly conditioned.

2.3. Data processing

Using *Fit2D*, 2D XRD patterns were reduced to one-dimension patterns of intensity versus 2θ. The 2D XRD patterns were integrated every 15° in the azimuthal direction from -7.5° to 352.5°. Each azimuthal sector represents scattering from lattice planes that are oriented at different angles to the electric field direction. For instance, the 0° azimuthal sector contains scattering from lattice planes that are approximately parallel to the electric field direction, while the 90° sector contains scattering from lattice planes that are perpendicular to the electric field direction [10].

To utilize the full information in the diffracted image, some of the symmetrically equivalent azimuthal sectors were summed, allowing the reduction of the 24 sectors to 7 azimuthal sectors that resemble the first quadrant of the 2D image. The first symmetry element in the image is that the top half of the image should be equivalent to the bottom half of the image through a mirror plane. This is attributed to the fact that the electric field is applied parallel to the detector (vertically) and, for Bragg diffraction, a horizontal mirror plane exists in the sample symmetry due to Friedel's law. The second symmetry element is a second mirror plane between the left and right side of the detector due to random in-plane orientations in the sample. These two symmetry

elements are represented in Fig. 4, relative to the 24 azimuthal sectors. To obtain a sector that is now referred to as the 0º sector, sectors 1 and 13 were averaged. Similarly, the 15º sector is the average of sectors 2, 12, 14, and 24. This method of averaging equivalent sectors enables use of data from the entire diffraction image and increases the signal to noise ratio in the resultant sectors.

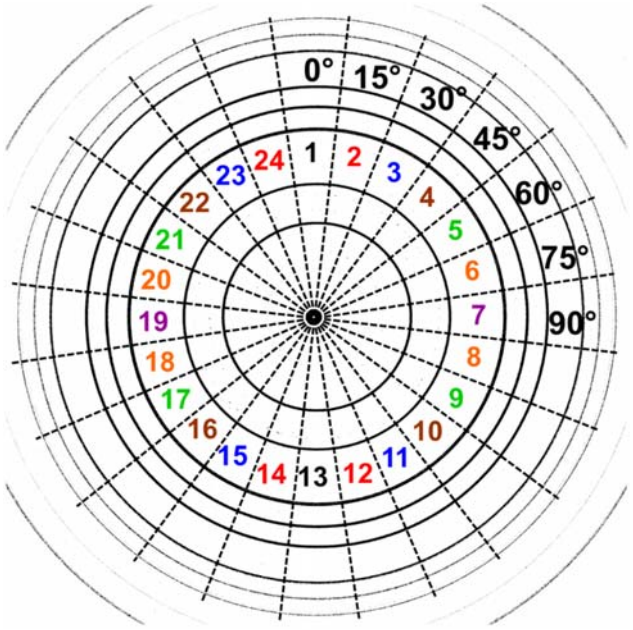

Fig. 4. Schematic representation of equivalent sectors from Bragg condition (top-bottom equivalency) and sample orientation (left-right equivalency) in 2D diffraction images.

2.4. Peak fitting analysis

The 002 and 200 degenerate reflections were fit using line profile analysis. The asymmetric nature of the peaks cannot be adequately fit using symmetric profile shape functions. Only the symmetrical portion of the asymmetric peaks were fit to profile shape functions. This was accomplished by using the outer intensities of each respective peak (e.g. low 2θ side of the 002 reflection) and assuming that this half of the peak is equivalent to the symmetric portion of the other half of the peak. This assumption and approach are justified because the asymmetry is mostly

attributed to the presence of ferroelastic domain walls themselves [11]. In contrast, the motion of domain walls is represented in the variation in reflection intensities and is the subject of the present work. A symmetric Pearson VII profile function [12] was used in the fitting. Fig. 5 illustrates that this profile function fits well to the lower 2θ side of 002 (blue circles) and the upper 2θ side of 200 (red circles). The lattice strain was obtained from the shift in the peak position at different electric fields. The extrinsic contribution related to the 90° domain wall motion was obtained from the variation of the integrated intensities of the 002 and 200 peaks as described in the subsequent section.

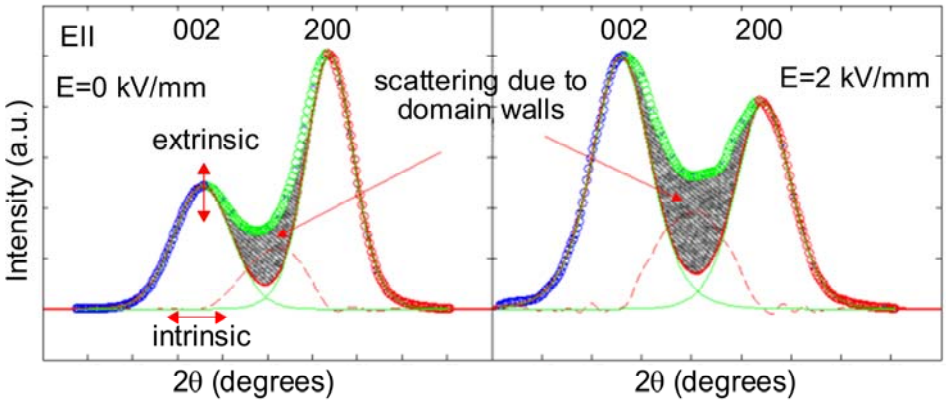

Fig. 5. Peak data processing. Two symmetric PVII functions (green lines) are created from lower and upper 2θ peaks (blue and red circles). The shaded grey regions related to the scattering due to domain walls are calculated subtracting the experimental data (all circles) from the sum of PVIIs (red continuous line). The dashed red line are obtained as a result of the subtraction.

2.5. Intrinsic contribution: electric-field-induced lattice strain

To estimate the lattice strain contribution $\varepsilon_{zz}^{lattice}$ to the macroscopic strain we followed the approach introduce by Daymond [13] assuming that the polycrystalline material under analysis only presents ferroelastic domain texture f_{hkl}, and no crystallographic texture. This assumption entails to calculate $\varepsilon_{zz}^{lattice}$ from a weighted average of the electric-field-induced lattice strain $\varepsilon_{hkl}^{E}(\alpha)$ for the individual *hkl* lattice planes according to Ehmke *et al.* [14]:

$$\varepsilon_{zz}^{lattice} = \frac{\sum_{hkl} f_{hkl}(\alpha=0) m_{hkl} \varepsilon_{hkl}^{E}(\alpha=0)}{\sum_{hkl} f_{hkl}(\alpha=0) m_{hkl}} \quad (1)$$

In Eq. (1), m_{hkl} are the multiplicities of the peaks and $\varepsilon_{hkl}^{E}(\alpha)$ was calculated from

$$\varepsilon_{hkl}^{E}(\alpha) = \frac{d_{hkl}(\alpha) - d_{hkl}^{0}}{d_{hkl}^{0}} \quad (2)$$

where d_{hkl} is the inter-planar d-spacing for a specific *hkl* plane and the superscript 0 indicate the d-spacing for zero electric field.

To perform the f_{hkl} calculation for subsequent use in the Eq. (1), the pseudo cubic reflections 110 and 200 were taken into account. The f_{002} and f_{200} were calculated from [14]:

$$f_{002}(\alpha) = \frac{3\frac{I_{002}(\alpha)}{I_{002}^{unpoled}}}{\frac{I_{002}(\alpha)}{I_{002}^{unpoled}} + 2\frac{I_{200}(\alpha)}{I_{200}^{unpoled}}} \quad (3)$$

and

$$f_{200}(0) = \frac{3}{2} - \frac{f_{002}(0)}{2} \quad (4)$$

Due to the small aspect ratio of the crystal, no splitting could be seen in the 110 reflection, although 101 and 110 peaks have different lattice spacing. In this case it is possible to assume $\varepsilon_{101}(0) = \varepsilon_{110}(0)$ and $f_{101} = f_{110} = 1$ [14]. Here, the contribution of the 111 reflection to lattice strain was not taken into consideration given the shift of the peak position with the applied electric field is negligible compared to 100 and 110 peaks shift. Fig. 6(a) shows the lattice strain–electric field hysteresis loop obtained from this analysis approach. The comparison for the electric field induced lattice strain and the macroscopically measured electric field induced strain is shown in Fig. 6(b).

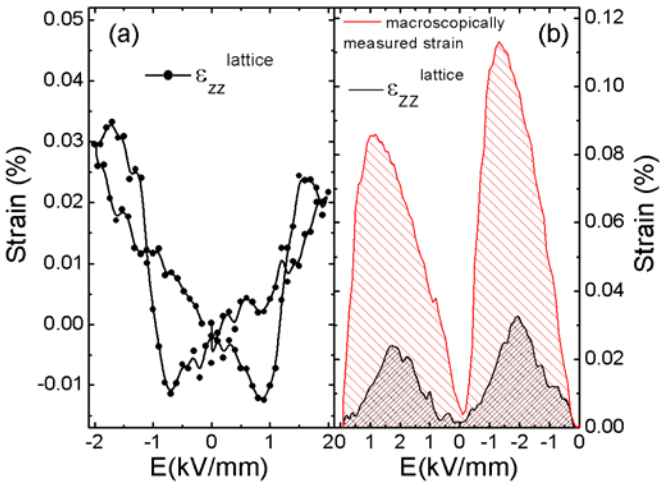

Fig. 6. (a) Electric field induced lattice strain versus the electric field at an angle parallel to the applied electric field and (b) comparison to the macroscopically measured electric field induced strain.

2.6. Extrinsic contribution: domain wall motion

In poled polycrystalline piezoelectric materials, grains of all orientations contribute to the longitudinal macroscopic strain ε_{zz}^{total} parallel to the direction of the applied electric field. Non-180° reorientation creates an anisotropic dimensional change in the material, which is associated with the reorientation of spontaneous strain in the lattice. The crystallographic spontaneous strain S_t for a tetragonal crystal is given by:

$$S_t = \frac{d_{00l} - d_{h00}}{d_{h00}} \tag{5}$$

where d_{hkl} is the interplanar d-spacing for a specified *hkl* plane.

The contribution due to non-180° domain switching, in an individual grain, is a function of the grain orientation with respect to the direction of the applied electric field. The overall contribution of non-180° domain switching $\varepsilon_{zz}^{extrinsic}$ can be calculated from *in situ* XRD patterns of all azimuthal sectors from 0º to 90º. The anisotropic strains of all the grains are projected to the sample direction (parallel to electric field) by performing a weighted sum of the projected strains

[15]. The weighted sum accounts for the volume fraction of differently oriented grains. The $\varepsilon_{zz}^{extrinsic}$ is given by:

$$\varepsilon_{zz}^{extrinsic} = S_t \int_0^{\pi/2} [m\Delta\eta(\alpha)\cos^2(\alpha)] \sin(\alpha)\, d\alpha \tag{6}$$

being m=3 for tetragonal crystallographic structure.

The geometrical factor $\cos^2(\alpha)$ projects the strain induced by domain switching in the direction of the applied field, where α is the sector angle. The term $\Delta\eta$ represents the change in volume fraction of the non-180° domain switching with applied electric field between the zero volt pattern and a non-zero volt pattern. The factor $m\Delta\eta$ accounts for the domain reorientation within the sample. The factor sin(α) describes the transformation from a volume in the orientation space to an effective volume fraction within the sample [16].

To determine the change in volume fraction of the non-180° domain switching, the domain reorientation must be quantified. The volume of switched domain η_{002} was calculated from the integrated intensities of the 002 and 200 by using Eq. (7). The integrated intensities were obtained from a line-profile analysis [17].

$$\eta_{00h}(\alpha) = \frac{\frac{I_{00h}(\alpha)}{I_{00h}^{unpoled}}}{\frac{I_{00h}(\alpha)}{I_{00h}^{unpoled}} + 2\frac{I_{h00}(\alpha)}{I_{h00}^{unpoled}}} - \frac{1}{3} \tag{7}$$

In Eq. (7), $I_{00h}^{unpoled}$ is the integrated intensity of the 00h reflection of the sample in its unpoled state and $I_{h00}(\alpha)$ is the integrated intensity of the 00h reflection at a specified voltage and sector α.

In order to compare the strain obtained from the XRD data processing to the macroscopically measured strain, the total strain obtained from XRD was computed as:

$$\varepsilon_{zz}^{total} = \varepsilon_{zz}^{lattice} + \varepsilon_{zz}^{extrinsic} \tag{8}$$

3. Results and Discussion

Fig. 7(a) shows the contour plot of the 200 reflections from the 0º sector, which contains scattering vectors that are oriented approximately parallel to the electric field. The contour plot shows XRD data that represents switching of *a*-oriented domains to *c*-oriented domains that can be quantified by Eq. (3) from integrated intensities values of the 1-D patterns. 1D patterns are extracted from Fig. 7(a) and shown in Fig. 7(b) in order to compare data obtained at different electric field amplitudes of -2, 0, and 2 kV/mm. The difference in intensities of the peaks within the 1D patterns is proportional to the amount of domain switching. The amount of 90° domain switching within a grain is highly dependent on the orientation of that grain within the sample. The amount of domain switching decreases from sector 0º to 90º. This is due to the orientation of the grains that are being probed within each sector relative to the applied electric field direction. Fig. 7(c) illustrates this trend by showing the degree of 90º domain reorientation, η_{002}, as a function of angle to the applied electric field. With increased angle, η_{002} decreases smoothly. Negative values of η_{002} indicate that there are dominantly *a*-oriented domains versus *c*-oriented domains, which is expected in the 90° sector.

Fig. 8 shows the comparison between the values of the macroscopically measured strain and the total strain ε_{zz}^{total} obtained from XRD data processing. It is observed that for positive values of the applied electric field both match fairly well. In the other hand, for the negative values of the applied electric field a slight mismatch is observed. This mismatch could result from a difference in the applied frequencies between the macroscopic measurement and the *in situ* XRD measurement (0.1 Hz and 0.0125 Hz, respectively). Nevertheless, the most important result showed in Fig. 8 is that the major contribution to the total strain is due to the extrinsic contribution, $\varepsilon_{zz}^{extrinsic}$. This result is supported by Fig. 6, which shows minor contribution of field-induced

lattice strain. Overall, these results demonstrate that the majority of the macroscopic strain measured in the KNN-modified tetragonal polycrystal is due to non-180° domain wall motion.

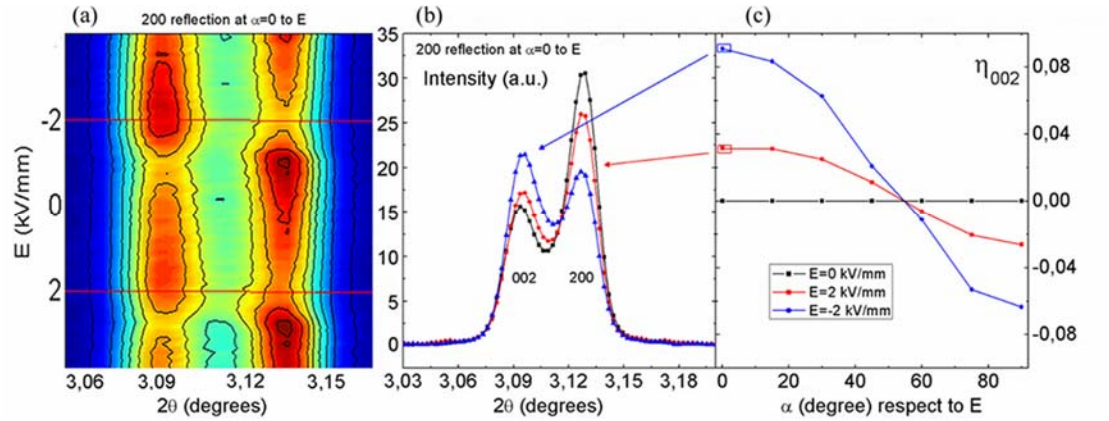

Fig. 7. (a) 200 reflections contour plot during the application of the electric field. Switching domains are represented by intensity differences. (b) Analysis of domain switching by comparing the peaks intensity for different electric fields applied. (c) Domain switching (η_{002}) as a function of angle to the applied electric field. Each point of η_{002} plot is obtained from the integrated intensities of their corresponding 002 and 200 degenerate reflections using Eq. 3.

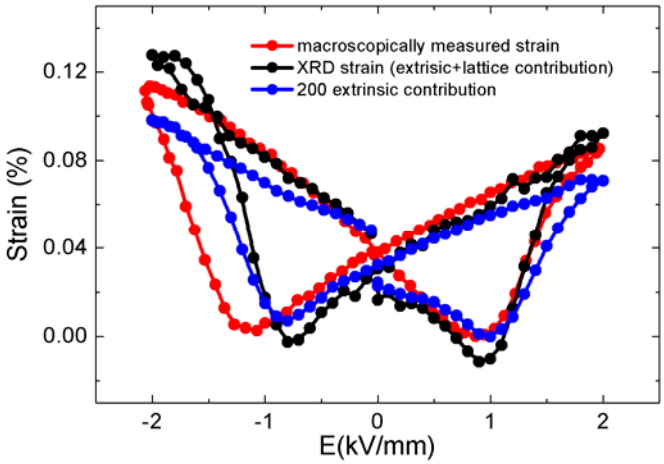

Fig. 8. Strain versus electric field loop obtained from macroscopic measurement (black), adding the XRD data processing from all the contributions (red), and from the 200 reflection contribution (blue).

Intrinsic and extrinsic contributions to piezoelectric and dielectric properties can also be studied using other approaches, for instance by measuring property coefficients as a function of temperature [18]. This approach take into account that the intrinsic contribution is the only response expected at very low temperatures, and it may be considered temperature-independent in temperature ranges that are sufficiently far from phase transitions. Thereby, this approach allows distinguish between the very low temperature response (intrinsic contribution) and the room temperature response (extrinsic plus intrinsic contributions). This alternative approach was previously performed in a similar KNL-NTS composition [19]. The results of the previous study indicate that variation of these responses in temperature shows the piezoelectric and dielectric coefficients increasing 3.5 and 7 times respectively from 20K to room temperature. Despite this work did not take into account the changes in the intrinsic contribution that are expected due to phase transitions, as the one that appears in the studied composition, it proves that the extrinsic contribution increase with increasing temperature for a fixed crystal structure. Furthermore, the same report also studies the responses of the compliance s_{11}^{E} and the piezoelectric coefficient d_{31}versus an applied electric field showing a predominant non-linear behavior associated to the domain wall motion at room temperature [19]. The remarkable advantage of the approach applied in the present work is that allow discerning between intrinsic and extrinsic contributions even in the temperature range where the phase transition occurs.

Previous work has shown that the domain wall motion in orthorhombic Li-modified KNN increases as the compositions closer to the polymorphic phase boundary (PPB) [20]. This prior observation in other KNN-based system is consistent with the present result in which a large extrinsic contribution is found in a tetragonal composition in close proximity to the PPB. This is similar to what has previously been observed in PZT from property measurements [21] and *in situ*

XRD measurements [15]. In a previous work by Pramanick *et al.* [17], a study of the structural changes in commercial PZT ceramics under the application of electric fields have been carried out. An enhancement of the piezoelectric response as large as 55% was found at relatively low applied electric field (0.75 KV/mm). Besides, increases of 300% in the real component of the dielectric permittivity under applied electric field (0.3 kV/mm) at temperatures of 400 K have been measured in PNZT [22]. That increase, mostly related to extrinsic contribution, shows the predominance of the extrinsic contribution in lead-based compositions. The results of the present work illustrate that extrinsic contribution in the form of non-180° domain wall motion is the primary contributor to the properties of lead-free KNN systems.

4. Conclusions

High-energy X-ray diffraction data analysis is a useful tool to achieve information regarding the relative contribution of intrinsic and extrinsic effects to the electromechanical response of polycrystalline piezoelectrics. The non-180° domain reorientation of the KNL-NTS piezoceramic is quantify from the integrated intensities of the 002 and 200 reflections obtained from line profile, while the shifts in peak position versus the applied electric field is used to obtain the lattice strain contribution. The comparison between the macroscopically measured strain and the total strain obtained from the XRD data processing match fairly well. The confirmation that the macroscopic strain is mainly driven by the extrinsic contribution related to the non-180° domain wall motion is obtained here from a different approach. However, the results are consistent with other approaches performed in previous works. The data processing employed in this work is, to the best of our knowledge, the only method allowing a direct separation of lattice and domain wall contributions to the electric field induced macroscopic strain in piezoelectric materials. The

method may represent a key point in order to gain insights in the design of new piezoelectric materials from domain engineering.

Acknowledgement

This work was supported by the MINECO (Spanish Government) project MAT2013-48009-C4-P. This research used resources of the Advanced Photon Source, a U.S. Department of Energy (DOE) Office of Science User Facility operated for the DOE Office of Science by Argonne National Laboratory under Contract No. DE-AC02-06CH11357. Dr. F. R-M is also indebted to MINECO for a ‘‘Juan de la Cierva’’ contract (ref: JCI-2012-14521), which is co-financed with FEDER funds.

References

[1] J. Rödel, K.G. Webber, R. Dittmer, W. Jo, M. Kimura, D. Damjanovic, Transferring lead-free piezoelectric ceramics into application, J. Eur. Ceram. Soc. 35 (2015) 1659–1681. doi:10.1016/j.jeurceramsoc.2014.12.013

[2] Y. Saito, H. Takao, T. Tani, T. Nonoyama, K. Takatori, T. Homma, T. Nagaya, M. Nakamura, Lead-free piezoceramics, Nature 432 (2004) 84–87. doi:10.1038/nature03028

[3] K. Uchino, Applications of lead-free piezoelectrics, in: S. Priya, S. Nahm (Eds.), Lead-Free Piezoelectrics, Springer, New York, 2012, pp. 511–528. doi:10.1007/978-1-4419-9598-8

[4] D. Damjanovic, A morphotropic phase boundary system based on polarization rotation and polarization extension, Appl. Phys. Lett. 97 (2010) 062906. doi:10.1063/1.3479479

[5] Q.M. Zhang, H. Wang, N. Kim, L.E. Cross, Direct evaluation of domain-wall and intrinsic contributions to the dielectric and piezoelectric response and their temperature dependence on lead zirconate-titanate ceramics, J. Appl. Phys. 75 (1994) 454. doi:10.1063/1.355874

[6] G. Tutuncu, L. Fan, J. Chen, X. Xing, J.L. Jones, Extensive domain wall motion and deaging resistance in morphotropic $0.55Bi(Ni_{1/2}Ti_{1/2})O_3$–$0.45PbTiO_3$ polycrystalline ferroelectrics, Appl. Phys. Lett. 104 (2014) 132907. doi:10.1063/1.4870506

[7] J.L. Jones, E.B. Slamovich, K.J. Bowman, Domain texture distributions in tetragonal lead zirconate titanate by X-ray and neutron diffraction, J. Appl. Phys. 97 (2005) 034113. doi:10.1063/1.1849821

[8] F. Rubio-Marcos, P. Ochoa, J.F. Fernandez, Sintering and properties of lead-free $(K,Na,Li)(Nb,Ta,Sb)O_3$ ceramics, J. Eur. Ceram. Soc. 27 (2007) 4125–4129. doi:10.1016/j.jeurceramsoc.2007.02.110

[9] A.P. Hammersley, FIT2D: An introduction and overview, ESRF Internal Report (1997) ESRF97HA02T.

[10] G. Esteves, C.M. Fancher, J.L. Jones, In situ characterization of polycrystalline ferroelectrics using X-ray and neutron diffraction, J. Mater. Res. 30 (2014) 340–356. doi:10.1557/jmr.2014.302

[11] J.E. Daniels, T.R. Finlayson, A.J. Studer, M. Hoffman, J.L. Jones, Time-resolved diffraction measurements of electric-field-induced strain in tetragonal lead zirconate titanate, J. Appl. Phys. 101 (2007) 094104. doi:10.1063/1.2720255

[12] J.E. Daniels, J.L. Jones, T.R. Finlayson, Characterization of domain structures from diffraction profiles in tetragonal ferroelastic ceramics, J. Phys. D. Appl. Phys. 39 (2006) 5294–5299. doi:10.1088/0022-3727/39/24/029

[13] M.R. Daymond, The determination of a continuum mechanics equivalent elastic strain from the analysis of multiple diffraction peaks, J. Appl. Phys. 96 (2004) 4263–4272. doi:10.1063/1.1794896

[14] M.C. Ehmke, N.H. Khansur, J.E. Daniels, J.E. Blendell, K.J. Bowman, Resolving structural contributions to the electric-field-induced strain in lead-free (1-x)Ba($Zr_{0.2}Ti_{0.8}$)O_3-x(Ba $_{0.7}Ca_{0.3}$)TiO_3 piezoceramics, Acta Mater. 66 (2014) 340–348. doi:10.1016/j.actamat.2013.11.021

[15] A. Pramanick, D. Damjanovic, J.E. Daniels, J.C. Nino, J.L. Jones, Origins of electro-mechanical coupling in polycrystalline ferroelectrics during subcoercive electrical loading, J. Am. Ceram. Soc. 94 (2011) 293–309. doi:10.1111/j.1551-2916.2010.04240.x

[16] J.L. Jones, M. Hoffman, K.J. Bowman, Saturated domain switching textures and strains in ferroelastic ceramics, J. Appl. Phys. 98 (2005) 024115. doi:10.1063/1.1988978

[17] A. Pramanick, J.E. Daniels, J.L. Jones, Subcoercive cyclic electrical loading of lead zirconate titanate ceramics II: Time-resolved X-ray diffraction, J. Am. Ceram. Soc. 92 (2009) 2300–2310. doi:10.1111/j.1551-2916.2009.03219.x

[18] Q.M. Zhang, H. Wang, N. Kim, L.E. Cross, Direct evaluation of domain-wall and intrinsic contributions to the dielectric and piezoelectric response and their temperature dependence on lead zirconate-titanate ceramics, J. Appl. Phys. 75 (1994) 454–459. doi:10.1063/1.355874

[19] D.A. Ochoa, J.E. García, R. Pérez, V. Gomis, A. Albareda, F. Rubio-Marcos, J.F. Fernández, Extrinsic contribution and non-linear response in lead-free KNN-modified piezoceramics, J. Phys. D. Appl. Phys. 42 (2008) 025402. doi:10.1088/0022-3727/42/2/025402

[20] T. Iamsasri, G. Tutuncu, C. Uthaisar, S. Pojprapai, J.L. Jones, Analysis methods for characterizing ferroelectric/ferroelastic domain reorientation in orthorhombic perovskite materials and application to Li-doped $Na_{0.5}K_{0.5}NbO_3$, J. Mater. Sci. 48 (2013) 6905–6910. doi:10.1007/s10853-013-7495-2

[21] D.J. Kim, J.P. Maria, A.I. Kingon, S.K. Streiffer, Evaluation of intrinsic and extrinsic contributions to the piezoelectric properties of $Pb(Zr_{1-x}T_x)O_3$ thin films as a function of composition, J. Appl. Phys. 93 (2003) 5568–5575. doi:10.1063/1.1566478

[22] J.E. Garcia, D.A. Ochoa, V. Gomis, J.A. Eiras, R. Pérez, Evidence of temperature dependent domain wall dynamics in hard lead zirconate titanate piezoceramics, J. Appl. Phys. 112 (2012) 014113. doi:10.1063/1.4736582